STATISTICAL FEATURE OF NON-DUCTED OMEGA SIGNAL AND ASSOCIATED ASE OBSERVED BY ISIS-I AND -II SATELLITES

Toshio MATSUO, Iwane KIMURA

Department of Electrical Engineering II, Kyoto University, Yoshida-Honmachi, Sakyo-ku, Kyoto 606

and

Hisao YAMAGISHI

National Institute of Polar Research, 9–10, Kaga 1-chome, Itabashi-ku, Tokyo 173

Abstract: Non-ducted Omega signals and associated ASE (Artificially Stimulated Emission) triggered by the Omega transmitter located at Aldra (66°25′15″N, 13°09′10″E, geographic) in Norway were observed by ISIS-I and -II satellites. During the period from May 30, 1976 to February 8, 1980, VLF data including Omega signals were obtained for 42 out of 642 passes. VLF emissions triggered by the Omega transmitter were detected only for 8 passes out of these 642 passes. Most of the 42 passes were observed within $\pm 15°$ of geomagnetic meridian through Aldra. Furthermore, the probability of the Aldra signal detection is relatively high in the daytime and for low *Kp* value mostly less than 3. In spite of the fact that Aldra is located in high latitude, the delay times of direct pulses to ISIS-I and -II satellites in the conjugate hemisphere were between 0.8 and 1.5 s in the *L* range of 2.4 to 4. The beginning latitude of each frequency component indicates that the frequency coincides with a quarter of minimum electron gryofrequency on a field line passing through the observing point.

1. Introduction

Since a high power VLF transmitter was installed at Siple Station in 1972, many controlled experiments of wave particle interactions in the magnetosphere have been performed using a conjugate ground station Roberval (HELLIWELL and KATSUFRAKIS, 1974; CARPENTER and MILLER, 1976), or satellites (INAN *et al.*, 1977; KIMURA *et al.*, 1981a, b; BELL *et al.*, 1981). One of the most remarkable differences of experiments using Siple transmission is that the transmitter frequency is lower than half of the frequencies of Omega transmissions and of the other navigation signals. Therefore, the Siple signals are more appropriate for probing more distant portion of the magnetosphere, *e.g.* from 3 to 6 in *L* shells, than Omega transmissions, whereas the signals from the Omega stations propagate in smaller *L* shell region, *e.g.* from 2.4 to 4.0.

So far, there were several ground observations of triggered emissions associated with relatively high frequency VLF transmissions. For instance, VLF emissions triggered by NPG (18.6 kHz) and NAA (14.4 kHz) signals were observed by HELLIWELL

et al. (1964). VLF emissions triggered by 1.0 s pulses from Omega low power ($\sim$100 W) transmitter located at Forest Port, New York were detected at Eights (KIMURA, 1968). CARPENTER *et al.* (1964) reported that triggering takes place most probably when the transmitter frequency is equal to half the minimum electron gyrofrequency along the field lines passing through the transmitter. On the other hand, as to satellite observations, Doppler shift phenomena observed by OGO-4 (WALTER and ANGERAMI, 1969), delay times measured by GEOS-1 (UNGSTRUP *et al.*, 1978), and ASE triggered by nonducted signals (BELL *et al.*, 1981) have been reported.

The purpose of the present paper is to report the results of ISIS-I and -II observation at Syowa Station, Antarctica, especially on the characteristic and statistic feature of propagation, and on triggered emissions of Omega signals transmitted from Aldra in Norway, and a comparison is made with previous works.

2. Omega Signal Format and Data Acquisition

Since May 30, 1976 in order to observe auroral hiss, VLF saucers and other ELF-VLF emissions, telemetry data acquisition of ISIS-I and -II satellites has been made at Syowa Station (69.1°S, 39.6°E; geographic) in Antarctica. We have paid special attention to Omega signals in regard to their ASE for the data from the beginning of the observation to February 8, 1980. It was found that the Omega signals transmitted from Aldra in Norway were observed for 42 out of 642 passes in total, and the triggered emissions were detected for 8 out of the above 42 passes. When the satellites were located within $\pm 15°$ of the geomagnetic meridian through Aldra, detection probability of the Omega signals increases up to 42 out of 325 passes.

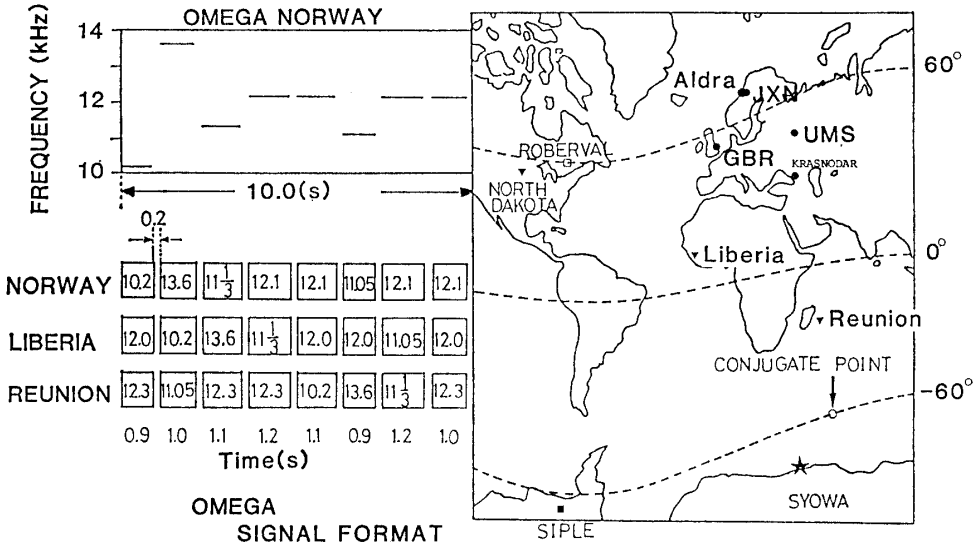

Fig. 1. Omega signal format, spectrum of signals from Aldra in Norway, and locations of related VLF transmitter stations and the conjugate point of Aldra.

Both Omega signals from Aldra observed by ISIS satellites and those from Liberia and Reunion observed on the ground (Syowa Station) were recorded on the same magnetic tape. To determine the absolute time of the received Aldra signals, which

propagated to the conjugate point from the source, we have made use of Liberia and Reunion signals based on the Omega signal format as shown in Fig. 1, so that the delay (propagation) time of the observed Aldra signals from the source can be determined. This format of the 10 s duration consisting of segments of various frequencies which characterize the transmitting station, is repeated. For example, 10.2, 12.0 and 12.3 kHz are transmitted from Aldra, Liberia and Reunion respectively in the same duration for the first 0.9 s of every 10 s from the hour at universal time. The Omega transmitter stations of interest and their magnetic conjugate points are marked in the world map shown in Fig. 1.

3. Statistical Feature of Observed Signals and Associated ASE

3.1. Spatial distribution of Omega signals and associated ASE

Figures 2a and 3a show all analyzed orbits of ISIS-I and -II, displayed on the equatorial planes, namely geomagnetic longitude *versus L* shell diagrams. In Figs. 2b and 3b, the portions of the orbit on which Aldra signals and their associated ASE were observed, are shown. The thick lines indicate intervals when triggered emissions were observed, and only Aldra signals observed are shown by thin lines. Since the geomagnetic meridian through Aldra lies at about 105°E, Omega signals and triggered emissions are

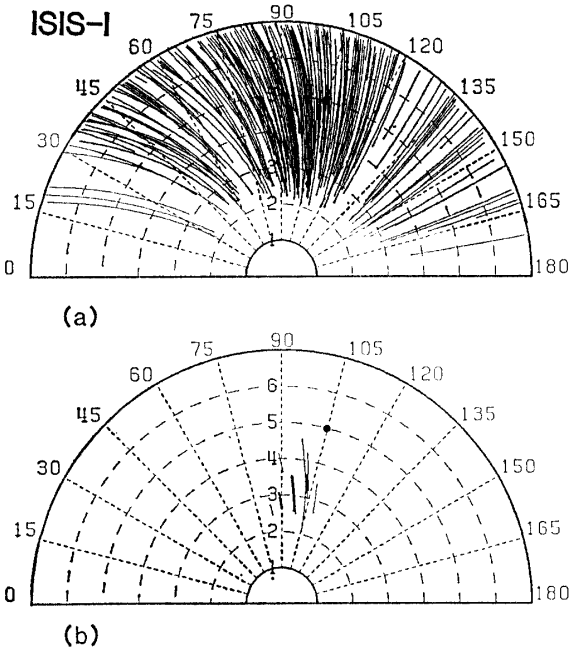

Fig. 2. *(a) All analyzed orbits of ISIS-I satellite displayed on geomagnetic equatorial plane, and the intersection with the equatorial plane of the magnetic field line through Aldra is indicated by a solid line.*
(b) The thin and the thick lines indicate the interval when signals from Aldra and ASE were observed by ISIS-I satellite respectively.

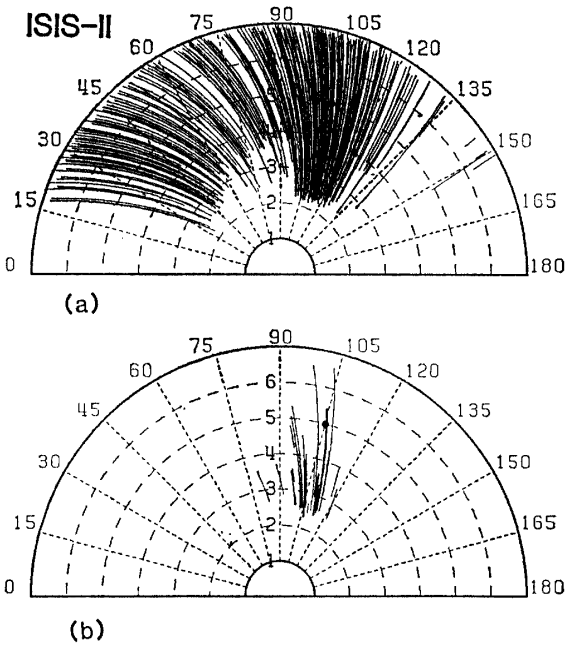

Fig. 3. *Diagrams for ISIS-II similar to those shown in Fig. 2.*

mostly observed when the satellites are located within $\pm 15°$ of this meridian as shown in Figs. 2b and 3b.

Statistical distribution of the paths on which the triggered emissions were observed, may indicate a region in the magnetosphere where the wave-particle interaction took place.

3.2. *Subsatellite local time and latitude dependence*

Figures 4a and 5a show subsatellite local time *versus* geographical latitude diagrams in which all passes observed by ISIS-I and -II satellites are plotted respectively. In (b) of both figures, the portions of these passes on which Aldra signals and Aldra-related ASE were observed were indicated by thin and thick lines respectively. Both Aldra signals and the triggered emissions show a tendency to be observed outside the dashed

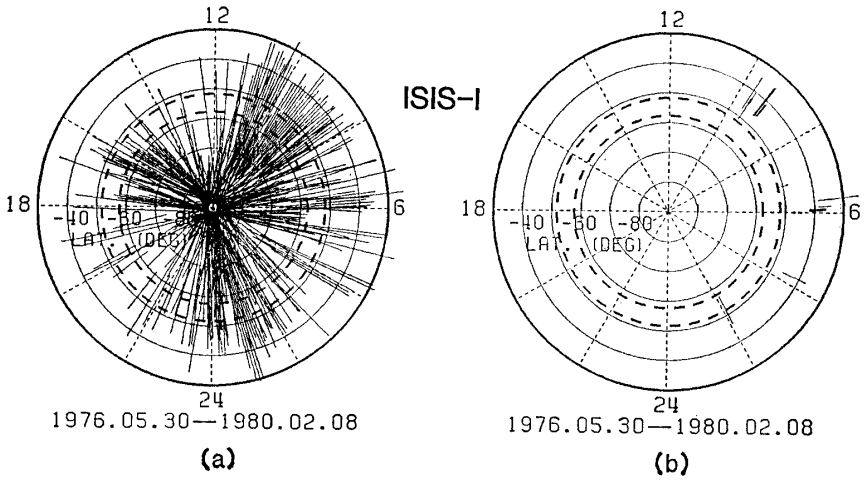

Fig. 4. *(a) All analyzed orbits of ISIS-I plotted in local time versus geographical latitude. (b) The thin and the thick lines indicate the intervals when signals from Aldra (thin lines) and ASE (thick lines) were observed by ISIS-I satellite. A circle of broken line corresponds to the conjugate latitude of Aldra at ISIS-I altitude 1400 km.*

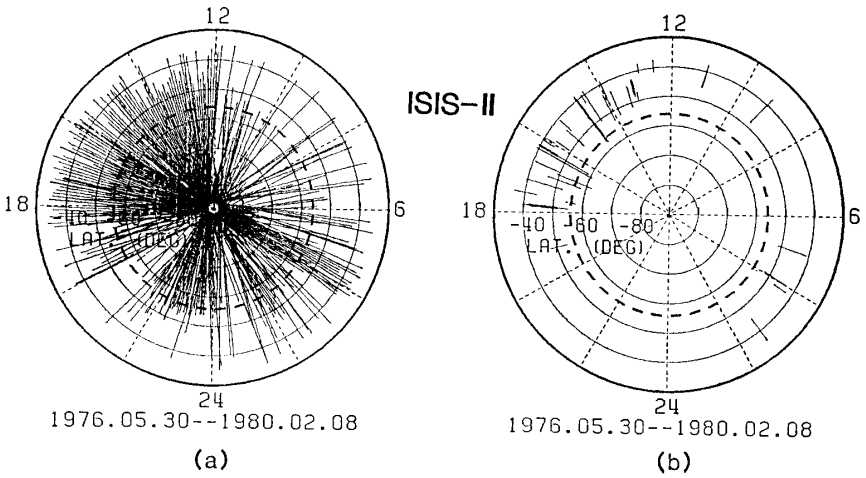

Fig. 5. *(a) Diagrams for ISIS-II similar to that shown in Fig. 4. (b) Two circles of broken line correspond to the conjugate latitude of Aldra, the satellite altitude, say 600 (inside circle) and 3500 km (outside circle).*

circles which denote the magnetic conjugate latitudes of Aldra station at the satellite altitudes (600 km (inside) and 3500 km (outside) for ISIS-I and 1400 km for ISIS-II). In other words, the signals are evidently received in an equatorward (or low latitude) region of the conjugate point. However, it must be noted that the number of ISIS-II orbits passing through the low L shell region is small for geomagnetic longitudes west-side the Aldra meridian.

3.3. Kp dependence

In Fig. 6a, a percentage of the number of satellite orbits for each *Kp* index against the total number of orbits is shown. A line represents the number of VLF received data for each *Kp* index. Non-hatched and hatched bar height show the occurrence probability of Aldra signals and their triggered emissions respectively. Occurrence probability of Aldra signals decreases with increasing *Kp* indices, but the number of the triggering cases is 2 for each *Kp* value between 0 and 3. On the other hand, averaged *Kp* for the maximum signal detection probability is almost the same as those in the previous works, for instance, ground observations (CARPENTER and MILLER, 1976; BELL *et al.*, 1981) and satellite observation (BELL *et al.*, 1981; INAN *et al.*, 1977).

It has been reported that the triggered emissions are generally detected under

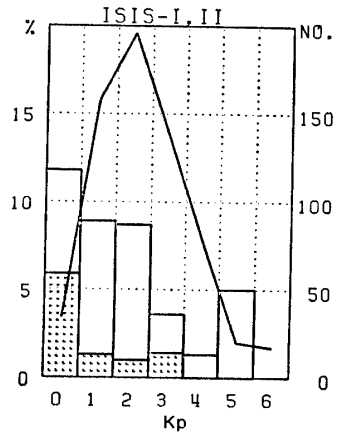

Fig. 6a. Non-hatched and hatched bar heights show the occurrence probability of Aldra signals and their triggered emissions respectively.

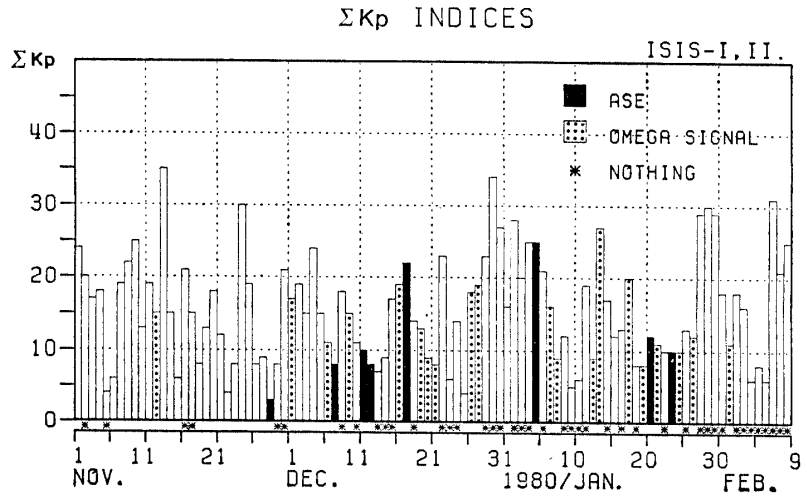

Fig. 6b. A line represents the number of VLF received data for each Kp index.

magnetic quiet conditions after magnetic disturbances (KIMURA *et al.*, 1981a, b). Our results have similar tendency except 2 cases on December 17, 1979 and January 4, 1980 as shown in Fig. 6b.

3.4. Comparison of our ISIS observation of VLF signals with previous works

It is interesting to compare the Omega signals observed by ISIS satellite with those of previous works on the signals observed by satellites or ducted signals observed on the ground. When ISEE-1 spacecraft was located within 30° of the geomagnetic meridian through North Dakota and Siple, then the percentage of reception of signals on the satellite was approximately 80 and 50% respectively (BELL *et al.*, 1981), and Explorer 45 and Imp 6 also show a similar tendency (INAN *et al.*, 1977). Moreover, the reception probability observed by ISEE-1 satellite in the vicinity of the equatorial plane for signals from North Dakota was approximately 80%. On the other hand, according to the present study using the ISIS satellite data, the ratio of the Aldra signal reception is 42 out of 325 passes (13%) when the satellite location was within $\pm 15°$ of the geomagnetic meridian passing through Aldra, which is located at a latitude higher than North Dakota.

4. Characteristics of Omega Signal Propagation

4.1. Spectra of Omega signals and associated ASE

We now show the representative spectra of the VLF signals observed by ISIS-II, as shown in Figs. 7 and 8. The spectrum in Fig. 7 was observed on January 4, 1980,

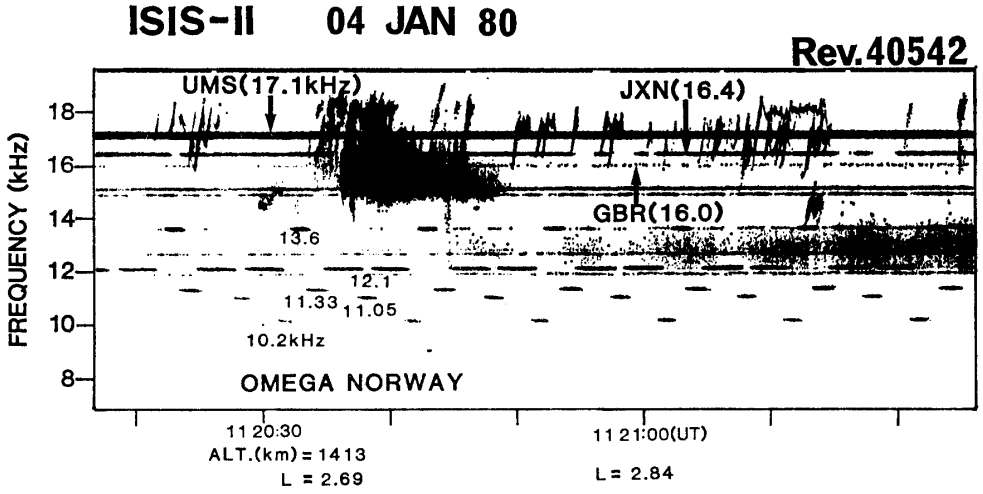

Fig. 7. Frequency-time spectrum of typical ASE observed by ISIS-II satellite. ASE triggered by 13.6 kHz Omega signal and UMS, JXN, GBR signals which are transmitted from west USSR, Norway (Helgeland: 66.4°N, 13.0°W), UK(Rugby: 52.4°N, 1.2°W) respectively are also seen.

in which a sequence of the frequency shift of 10.2, 13.6, 11.33, 12.1, 12.1, 11.05, 12.1, 12.1 kHz is shown (also see Fig. 1). *Kp* index at this time of observation was 3 and $\sum Kp$ was 25, and the satellite local time was about 14 LT. The pulses which were accompanied by ASE were only of 13.6 kHz Omega signal among 5 different frequencies transmit-

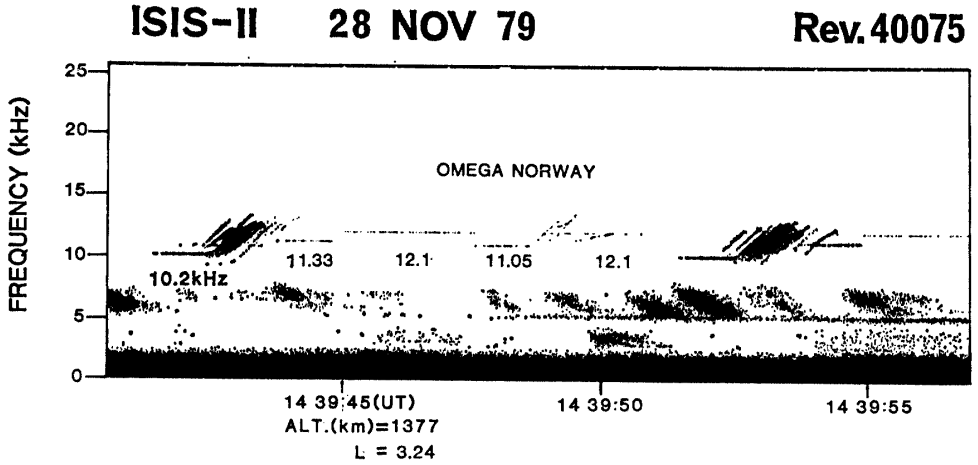

Fig. 8. Discrete riser type emissions triggered by 10.2 and 11.05 kHz signals composed of multipath structures.

ted from Aldra, and of other signals in the frequency range from 16 and 18 kHz. Spectra of typical Omega ASE observed by ISIS-I and -II satellites are composed of discrete riser emissions. On the other hand, as shown in Fig. 8, ASE's were triggered by 10.2 and 11.05 kHz signals among 5 Omega transmitter frequencies, and multipath structures of ASE are seen in the figure. *Kp* index at this time was 0 and ΣKp was 3, namely under a magnetically dead calm condition. The satellite local time was about 17 LT.

4.2. Measurement of delay time

It is important to measure the delay time of the signal from the source to the satellite, because it will give a clue to determine the propagation path to the satellite in the conjugate hemisphere.

As the delay time is proportional to the square root of the electron density, we could infer the electron density along the ray path, and also determine the mode of propaga-

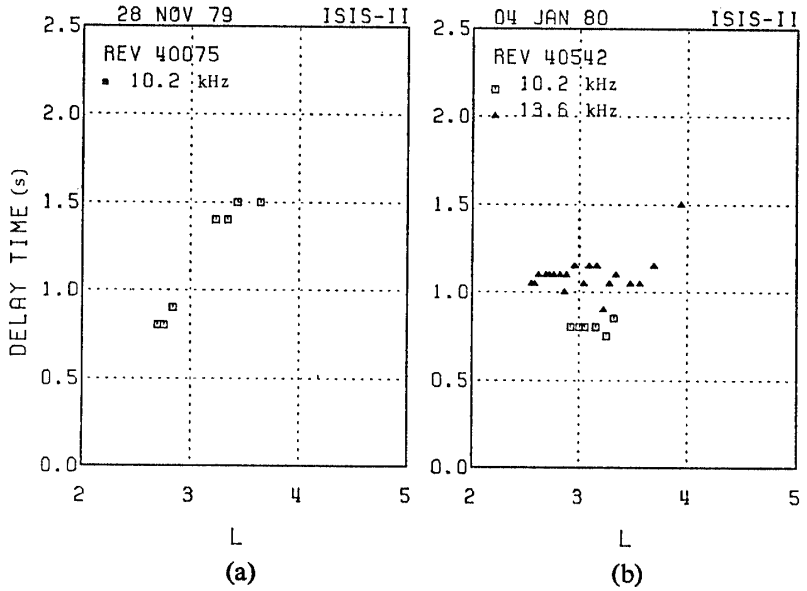

Fig. 9. Measured delay time for the signals from Aldra to satellite. (a) The delay time increases with increasing latitude of observation point. (b) The delay time is almost constant with latitudes.

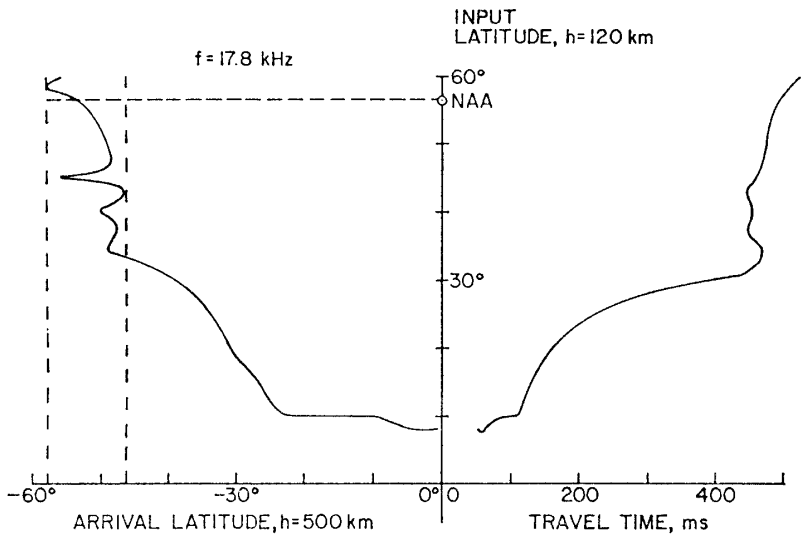

Fig. 10. Arrival latitude and corresponding delay times for waves of 17.8 kHz as a function of the input latitude in the northern hemisphere (after SCARABUCCI, 1969).

tion. There are two types of the delay time variation with latitude, that is, the one in which the delay time increases with increasing latitude of observation points as shown in Fig. 9a, and the other in which the delay time is almost constant with latitude as shown in Fig. 9b. The former is rather understandable characteristic, because usually the delay time changes smoothly as a function of latitude (BELL *et al.*, 1981). However the latter should be interpreted by rather peculiar propagation paths. For example, as was reported by SCARABUCCI (1969) a steep latitudinal gradient of electron density such like a trough will give rise to almost constant time delay over a range of arrival latitude (see Fig. 10).

4.3. Non-ducted propagation and a quarter $f_{H\,min}$ cut-off phenomenon

We present another interesting example of the Omega spectrum observed by ISIS-II satellite in Fig. 11, in which marked by arrows are different frequencies transmitted

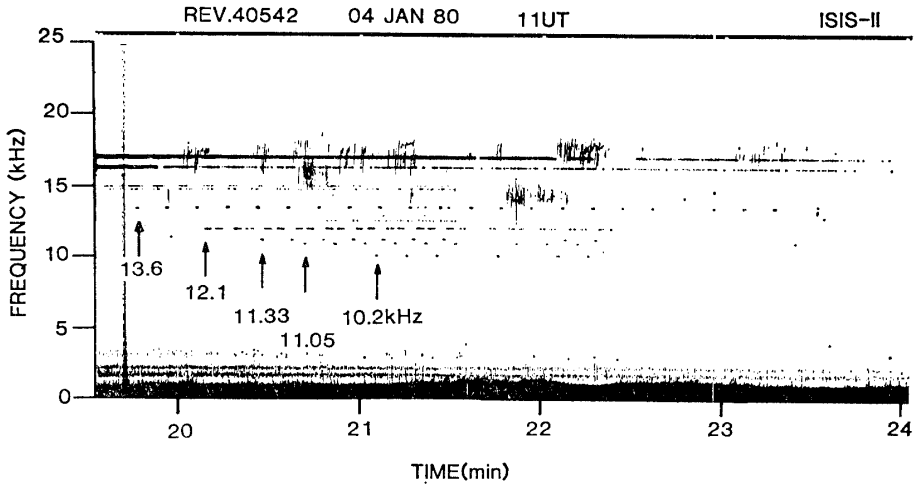

Fig. 11. When the satellite moves from middle to high latitude, in spite of the same transmitting station, the highest frequency component of the Aldra signals was first observed, and then lower frequency components were successively observed with delays.

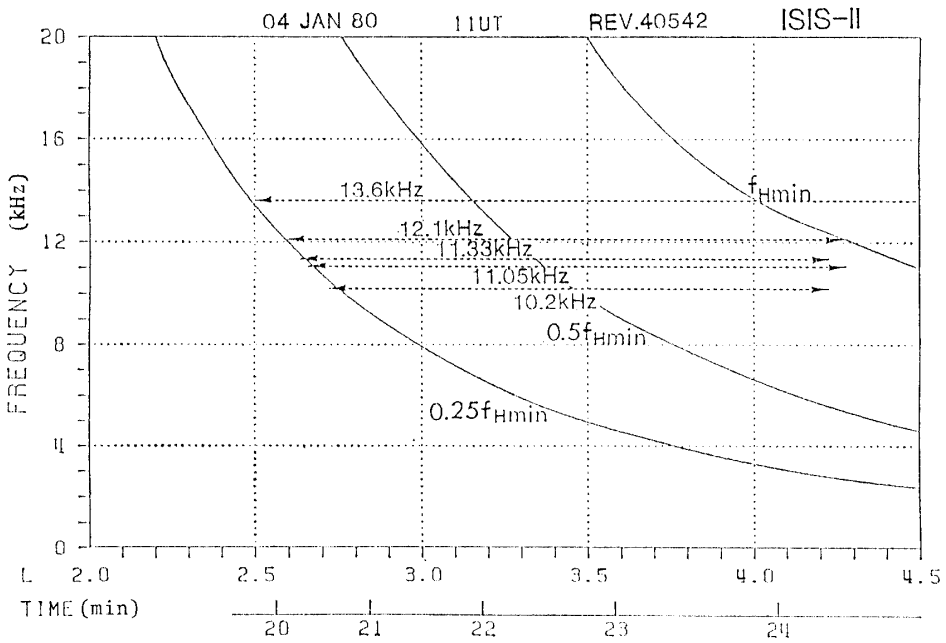

Fig. 12. The intervals in which Aldra Omega signals at 5 different frequencies were observed on ISIS-II are indicated by 5 dotted lines, and a clear cut off at the quarter of the $f_{H\,min}$ is seen for all frequency components of Aldra.

from the same station Aldra. As the satellite moves from middle to high latitude, the highest frequency was first observed, and then lower frequency components were successively observed with delays. This situation is illustrated in Fig. 12, where the minimum electron cyclotron frequency ($f_{H\,min}$) along a field line calculated by IGRF 1975 model is also shown with time and L value. In the figure we also show the intervals between the beginning and the end time of the signals detected at the satellite for the 5 transmitted frequencies, and a clear cut-off at the quarter of the $f_{H\,min}$ is seen for all frequencies of Aldra. The observed range in L shells was from 2.5 to 2.72. The reason of this interesting $1/4\,f_{H\,min}$ cut-off characteristic is not clear and is now under study. Moreover, if the signals from Aldra had propagated along a field-aligned duct, these frequencies must be less than half the $f_{H\,min}$. Actually, however, the signals were observed on ISIS-II over a wide range where the signal frequency lies between a quarter of $f_{H\,min}$ and $f_{H\,min}$. It means that the propagation paths to the satellite in the conjugate hemisphere cannot be a ducted propagation.

5. Discussion and Conclusions

Among VLF spectral data observed by ISIS-I and -II in the past 4 years from 1976 to 1980, we have picked up those in which Omega signals transmitted from Aldra, Norway were detected. The results of our study indicate that the Omega signals and the associated ASE were mostly observed in a magnetically calm condition. These characteristics are similar to those resulted from the previous works. However, the probability of the signal and ASE detection was much lower than those obtained by other satellites which observed Omega and Siple signals. The reason for this may be as follows.

The ratio of the transmitted frequency (f) to $f_{H\,min}$, namely, $f/f_{H\,min}$ at North Dakota for ISEE observation was in the range of 0.5 to 0.7, so that it is possible for the signals to propagate to the spacecraft after crossing the equatorial plane by non-ducted propagation. On the other hand, in our case the above ratio is beyond 1.5, so that it is not easy for the signal to propagate to the conjugate hemisphere. Actually, the signals transmitted from Aldra can propagate to ISIS's in the southern hemisphere only in the condition that the electron density has a sharp latitudinal gradient, like a trough at high latitude. Under such a condition, the wave normal is strongly bent equatorwards at lower height, and then the signal can reach the satellite.

Acknowledgments

We are gratefull to Dr. E. BARRINGTON, Communications Research Center, Canada, NASA, U. S. A. and the ISIS Working Group for their support to the ISIS VLF observation at Syowa Station, Antarctica. We also thank the members of 17th, 18th, 19th and 20th wintering parties of the Japanese Antarctic Research Expedition for data acquisition at Syowa Station. The authors wish to thank Dr. R. FUJII of the National Institute of Polar Research for providing us the computer program for geomagnetic field line tracing in order to obtain conjugate point.

References

BELL, T. F., INAN, U. S. and HELLIWELL, R. A. (1981): Nonducted coherent VLF waves and associated triggered emissions observed on the ISEE-1 satellite. J. Geophys. Res., **86**, 4649–4670.

CARPENTER, D. L. and MILLER, T. R. (1976): Ducted magnetospheric propagation of signals from the Siple, Antarctica, VLF transmitter. J. Geophys. Res., **81**, 2692–2700.

CARPENTER, D. L., STONE, K. and LASCH, S. (1964): A case of artificially triggering of VLF magnetospheric noise during the drift of a whistler duct across magnetic shells. J. Geophys. Res., **74**, 1848–1855.

HELLIWELL, R. A. and KATSUFRAKIS, J. P. (1974): VLF wave injection into the magnetosphere from Siple Station, Antarctica. J. Geophys. Res., **79**, 2511–2518.

HELLIWELL, R. A., KATSUFRAKIS, J. P., TRIPI, M. and BRICE, N. (1964): Artificially stimulated VLF radiation from the ionosphere. J. Geophys. Res., **69**, 239.

INAN, U. S., BELL, T. F., CARPENTER, D. L. and ANDERSON, R. R. (1977): Explorer 45 and Imp 6 observations in the magnetosphere of injected waves from the Siple Station VLF transmitter. J. Geophys. Res., **82**, 1177–1187.

KIMURA, I. (1968): Triggering of VLF magnetospheric noise by a low power ($\sim$ 100 Watts) transmitter. J. Geophys. Res., **73**, 445–447.

KIMURA, I., MATSUMOTO, H., MUKAI, T., HASHIMOTO, K., HELLIWELL, R. A., BELL, T. F., INAN, U. S. and KATSUFRAKIS, J. P. (1981a): JIKIKEN (EXOS-B) observation of Siple transmissions. Adv. Space Res., **1**, 197–202.

KIMURA, I., MATSUMOTO, H., MUKAI, T., HASHIMOTO, K., HELLIWELL, R. A. BELL, T. F., INAN, U. S. and KATSUFRAKIS, J. P. (1981b): EXOS-B/Siple Station VLF wave-particle interaction experiment. Relation between Laboratory and Space Plasmas, ed by H. KIKUCHI. Dordrecht, D. Reidel, 331–338 (Astrophysics and Space Science Library, Vol. 84).

SCARABUCCI, R. R. (1969): Interpretation of VLF signals observed on the OGO-4 satellite. Tech. Rep. No. 3418–2, Stanford, Radio Sci. Lab., Stanford Univ.

UNGSTRUP, E., NEUBERT, T. and BAHNSEN, A. (1978): Observation on GEOS-1 of 10.2 to 13.6 kHz ground based transmitter signals. Space Sci. Rev., **22**, 453–464.

WALTER, F. and ANGERAMI, J. J. (1969): Nonducted mode of VLF propagation between conjugate hemisphere; Observations on OGO's 2 and 4 of the walking-trace whistler and of doppler shifts in fixed frequency transmissions. J. Geophys. Res., **74**, 6352–6370.

(Received May 10, 1982; Revised manuscript received October 18, 1982)